A study on supercritical water injection as waste heat recovery system in internal combustion engines

Applied Thermal Engineering 248 (2024) 123084

Contents lists available at ScienceDirect

Applied Thermal Engineering

journal homepage: www.elsevier.com/locate/apthermeng

Research Paper

A study on supercritical water injection as waste heat recovery system in internal combustion engines

Roberto Ianniello *, Michele Pipicelli, Giuseppe Di Luca, Carlo Beatrice, Gabriele Di Blasio

CNR –STEMS, via G. Marconi, 4, 80125 Napoli, Italy

ARTICLE INFO

Keywords:
Direct Water Injection
Super Critical Water Injection
Waste Heat Recovery
Natural Gas Engines
Efficiency
NOx reduction
Combustion process improvements

ABSTRACT

The rush towards solutions able to increase the sustainability of energy conversion systems in terms of efficiency and emissions is becoming even more significant in view of the transition to the zero-emission carbon target by 2050. In this context, waste heat recovery (WHR) is a possible solution to increase the systems global efficiency. In particular, the recovery of the high energy content from the exhaust has gained attention, especially for internal combustion engine applications. In the framework of WHR systems, a novel application of the concept is heating the water, as a working fluid, up to the supercritical condition to be injected directly into the combustion chamber to increase the cycle work. The approach includes the recovery of the needed water from the exhaust gases for closed-loop operations. To the authors' knowledge, no experimental studies have been published in the literature that investigate the feasibility of using supercritical water injection (SWI) in internal combustion engines. Specific WHR layout and SWI systems have been developed and integrated into a single-cylinder spark ignition engine. A proper experimental test campaign has been designed to assess the SWI potential on engine performance and emissions, and, as a supporting diagnostic tool, a quasi-dimensional model has been developed. The results evidence that although supercritical conditions have been reached in the heating system, the injection occurs in subcritical conditions because of the heat losses in the injector body. Direct water injection affects the combustion process in terms of heat release and charge cooling with effects on cycle work and NOx, depending on various factors such as water/fuel ratio (W/F) and injection timings. The technological limits of the integrated systems are discussed and supported by suited numerical studies, demonstrating that the theoretical advantages are not obvious and disclosing the possible solutions or strategies to improve the system performance.

1. Introduction

The energy conversion process from primary energy carriers to final energy use (mechanical power or electricity) involves several losses. A significant amount of energy is wasted as heat and needs to be recovered to raise conversion efficiencies [1]. Several studies on waste heat recovery (WHR) solutions have been published in the literature and proposing solutions to increase efficiencies in the various sectors such as mobility (down to −3% fuel consumption) [2], industrial and residential sectors (up to 34 % and 22 % of recoverable waste heat, respectively) [3]. As a sake of example, the wasted energy in the residential, industrial, commercial, and transport sectors in the United States is about 65 %, of which 22 % came from the transport sector [4]. In Europe, the industry wastes about 28 % of energy [5]. These results demonstrate a strong interest in conversion efficiency improvement through the use of effective WHR systems.

In the case of internal combustion engines (ICEs), despite future trends predicting its partial phase-out, they will likely continue to be adopted worldwide in the transport [6], agricultural [7], and energy generation [8] sectors. A relevant fuel energy share of ICE is wasted as heat through the exhaust gases (approx. 30–40 %), which can be partially recovered to increase the overall system efficiency [9]. In this context, the most studied WHR systems are thermoelectric generators (TEG) [10], mechanical or electrical turbo-compounding [11], organic Rankine cycle (ORC) [12], and Stirling cycles [13]. It has been estimated that a power generation of 500 W with a TEG WHR conversion efficiency of 4–5 % on a small vehicle in motorway driving conditions can lead to a carbon dioxide (CO_2) reduction of about 6–7 g/km [14]. Stobart et al. [15], considering the state-of-the-art technology of TEG WHR, have obtained benefits on fuel consumption of around 4 % for passenger cars and 7 % for heavy-duty vehicles, which shows the potential improvement of these technologies. However, the new system design and integration can increase complexity and weight. A study evaluating the

* Corresponding author.
E-mail address: roberto.ianniello@stems.cnr.it (R. Ianniello).

https://doi.org/10.1016/j.applthermaleng.2024.123084
Received 14 December 2023; Received in revised form 1 March 2024; Accepted 1 April 2024
Available online 3 April 2024

Nomenclature.

Abbreviations

APmax	Angle of peak pressure
AIC	Akaike Information Criterion
aTDC	after Top Dead Center
BIC	Bayesian Information Criterion
CA	Crank Angle
CA10-90	Combustion Duration
CA50	Crank Angle of 50 % of the total heat released
CFD	Computational Fluid Dynamics
CO_2	Carbon Dioxide
c_p	Specific heat capacity
DWI	Direct Water Injection
ECU	Electronic Control Unit
ET	Energizing Time
HRR	Heat Release Rate
HTC	Heat Transfer Coefficient
IAPWS	International Association for the Properties of Water and Steam
ICE	Internal Combustion Engine
IMEP	Indicated Mean Effective Pressure
isNOx	Indicated Specific NOx Emissions
LME	Linear Mixed-Effect
MAP	Manifold Air Pressure
NG	Natural Gas
NIST	National Institute of Standards and Technology
NOx	Nitrogen Oxides (NO, NO_2)
ORC	Organic Rankine Cycle
P_{cyl}	In-Cylinder Pressure
PFI	Port Fuel Injector
p_{rail}	Rail Pressure
Pmax	Peak Pressure
RNT	Russian National Committee
SA	Spark Advance
SCADA	Supervisory Control and Data Acquisition
SCE	Single-Cylinder Engine
SOI	Start of Injection
SWI	Supercritical Water Injection
TDC	Top Dead Center
TEG	Thermoelectric Generators
WHR	Waste Heat Recovery
W/F	Water/Fuel Ratio

Symbol

ρ	Density

impact of an ORC system on a light-duty commercial vehicle shows a penalty of 1 % in fuel consumption, due to the increase in the vehicle curb weight and higher engine back pressure [16].

WHR applications in ICE using water as a working fluid are widely studied, in liquid and gaseous phases. Different applications can be drawn from the literature, such as ICE-based cogeneration systems in which water thermodynamic conditions are generally at relatively high temperatures and low pressures and used as thermal vectors for industrial or residential applications [17]. On the other hand, there are studies regarding the effect of water injection in the combustion chamber heated through engine cooling circuits or exhaust gases. For instance, Liu et al. proposed a numerical study applying steam water on a natural gas (NG) engine, resulting in an efficiency improvement of up to 6.6 % [18]. Conklin and Szybist [19] studied the effect of water steam at 100 °C in a six-stroke ICE through a theoretical analysis, resulting in 25 % higher cycle work compared to the conventional four-stroke engine. Water direct injection at 120 °C has also been applied on an oxyfuel engine, showing about 8 % higher indicated work but alternating cycles with and without water injection [20]. To avoid possible interaction with combustion some numerical study as [21] reserve one cylinder of a multi-cylinder engine for water steam expansion. The theoretical reasoning behind the potential increase in work or efficiency is, to the authors' knowledge, not confirmed experimentally, and this study has the aim to provide a deeper experimental understanding of its feasibility.

In cases where there is more heat available from the exhaust gases, the water temperature can also be raised above the critical temperature (>374 °C) through a properly designed heat exchanger. Furthermore, specific high-pressure pumps can increase the pressure above the critical threshold (22.1 MPa). In the supercritical region, the fluid exists as a single phase and in an intermediate liquid-gaseous state [22], with notable differences in thermodynamic properties around the critical point. The reasonably higher density compared to the vapor phase allows the adoption of standard high-pressure liquid fuel injectors. Very few studies on water injection application in supercritical conditions have been published. Cantiani et al. performed preliminary studies of supercritical water for energy recovery through a Computational Fluid Dynamics (CFD) model. The analysis estimated a potential efficiency gain, with water injection at 35 deg after Top Dead Center (aTDC), of about 13 % compared to the reference case [23]. However, these concepts have not been verified in real applications, and to the authors knowledge, no experimental results on state-of-the-art engines are available. A proper experimental method applying supercritical water injection in a SI ICE was developed to exploit its energy content in seeking cycle work improvements. In most studies, water is applied in subcritical state, while in this manuscript the water is energized, increasing pressure and temperature up to the supercritical state. The proof-of-concept study was carried out experimentally on a single-cylinder engine to avoid constraints and compatibility issues related to multi-cylinder applications (turbocharger, after-treatment system, etc.). A proper WHR system was designed and integrated to recover the water and the heat from the exhaust gases. The feasibility of such a system has been studied and analyzed together with the effect on the combustion process of direct injection of water. The methodology and the tools defined for the experimental and numerical activities are described in section 2. The WHR performances and the combustion process analysis with Supercritical Water Injection (SWI) are presented in section 3. In particular, the numerical assessment of the integrated system is described in section 3.1. The experimental parametrization of the water quantity and timing and their effect on the combustion process, cycle work, NOx emissions and energy breakdown are discussed (3.2). A further analysis through a statistical approach is also conducted.

2. Materials and methods

This study aims to prove experimentally the potential advantages of supercritical water injection in an ICE. Therefore, it is worth clarifying its thermodynamic characteristics propaedeutically to the subsequent experimental setup design. First, the purpose is to exploit the energy content of the water, energized through the WHR system, and injected into the combustion chamber. Analysing the two potential thermodynamic transformations shown in Fig. 1.

Preparation of AF-PDES-GO-x/N, states A and B represent the initial condition of water at 40 °C and pressure of 50 and 300 bar, respectively. Final stages before injection are represented by A' and B', which is attained through isobaric transformation up to the temperature of 374 °C. It can be observed that the water density of condition B' is significantly higher than A', making traditional injectors, which operate

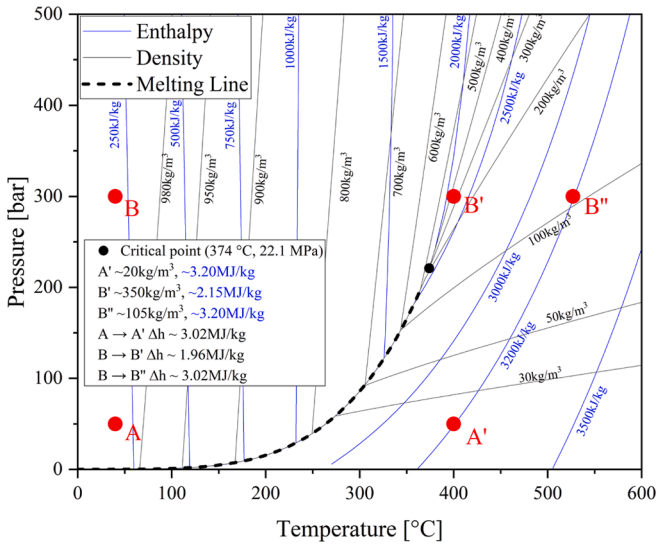

Fig. 1. Water enthalpy and density iso-curves on the p-v thermodynamic diagram.

with liquid fluid, a feasible option for this application. Furthermore, it is observed that the transformation B-B' requires less energy or enthalpy (~2 MJ/kg) than state A (~3 MJ/kg). Hypothesizing, constant the available heat and around 3 MJ/kg, the transformation at 300 bar, lead to a higher final temperature B'' (~527 °C) than B', with potentially better lower cooling effect when injected into the combustion chamber with benefits in terms of net work of the thermodynamic cycle.

To face with the application of the supercritical water injection concept, this study aims at developing an integrated engine and WHR setup to replicate the theoretical closed loop concepts, mentioned above, on the single cylinder engine (SCE). The schematic layout of the experimental setup to be developed is reported in Fig. 2. The water is pressurized in the range 221–300 bar through a high-pressure pump. Then, the pressurized water is heated up, exploiting the high-temperature exhaust gases through a heat exchanger. The water in supercritical conditions is directly injected into the combustion chamber during the combustion process. To close the loop, the exhaust gases pass through a condenser and water separator to recover the needed water for the injection.

To better clarify the various steps of the activity conducted, Fig. 3 reports a schematic workflow of the research activities performed. The mutual dependencies of the experimental, numerical, and statistical techniques are highlighted, and discussed in the following subsections. The first (2.1), describes the SCE, the integrated WHR and water injection systems. The second (2.2) illustrates the numerical quasi and one-dimensional models of the integrated SCE with the WHR for diagnostic and estimation purposes. The model validation was performed according to the test matrix of section 2.3 while results are reported in section 3.1.1.

2.1. Experimental setup

An experimental test matrix was properly designed and performed to

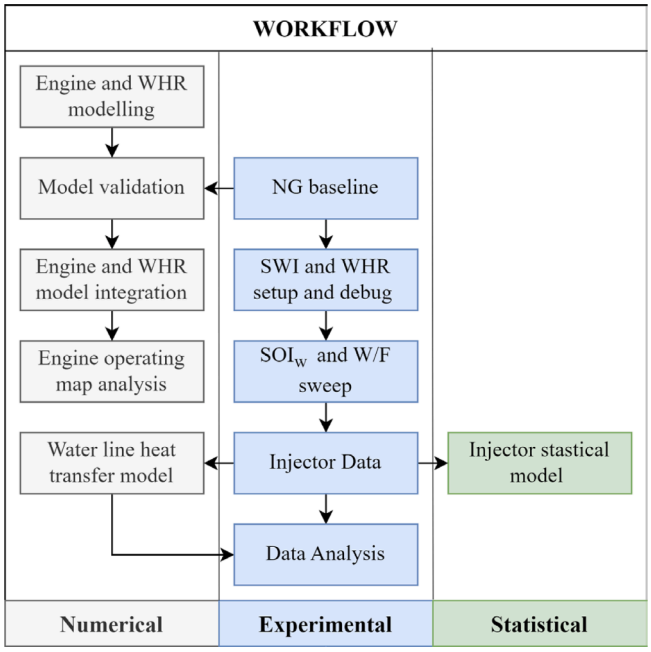

Fig. 3. Workflow of the research activities.

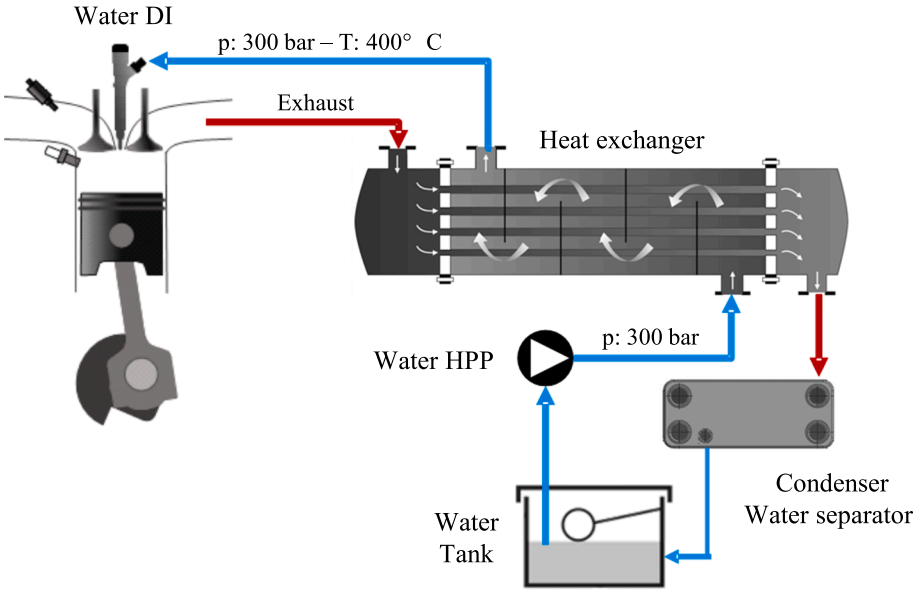

Fig. 2. Closed loop direct water injection concept.

assess the effects and possible drawbacks of applying the SWI concept. It has been applied on a naturally aspirated spark ignition SCE. A compression ignition cylinder head was appropriately modified to install the direct water injector and the spark plug. A diesel-derived injector was employed for the SWI. A solenoid-driven natural gas (NG) Port Fuel Injector (PFI) was mounted on the intake runner and closed the intake valve, for the purpose of NG injection. The spark plug was installed in a properly re-machined glow plug hole. The NG operating pressure was set at 8 bar through a proper pressure regulator. Table 1 provides a summary of the engine technical specifications.

The SCE experimental setup was chosen thanks to greater flexibility compared to multicylinder application, in terms of engine boundary condition, including intake, fuel, cooling, and lubricant, independently of the engine operating point. The engine control settings and auxiliary systems are managed through an open-loop electronic control unit (ECU) and a Supervisory Control and Data Acquisition (SCADA) system employing a National Instrument Platform. The in-cylinder pressure was measured using a flush-mounted piezo-electric Kistler 6053C pressure transducer, installed in a specially made hole through the cylinder head. The pressure signals have been recorded for 256 consecutive cycles with a 0.1 crank angle degree resolution and then averaged for the combustion process analysis. The NG mass flow was quantified through the thermal sensor Brooks SLA5863, while an AVL 733 gravimetric balance was used to record the water mass flow. The NOx exhaust emissions were analysed using a Smart NOx sensor. Other emissions are neglected in this first experimental campaign to avoid excessively contaminating the emission test bench with the high quantity of water at the exhaust, risking damaging the analyzers. Future activities will consider installing specific separators before the emission test bench. The developed experimental layout comprehensive of the WHR and water injection systems is depicted in Fig. 4.

As mentioned, the water injection, heating, and condensing systems have been developed to be integrated with the SCE and can pressurize the fluid up to 300 bar, through a high-pressure pump derived from the c4mmercial gasoline high-pressure pump. A closed-loop control unit has been developed to manage the injection pressure. The efficiency of the water heating system was dependent on the energy content of the exhaust gases. The supercritical fluid is directly injected into the combustion chamber through an appropriately modified direct-water injector. Fig. 5 shows a three-dimensional rendering of the direct water injector and the metal insert used for supercritical water adduction. The water injector, mounted on the head in the position of the conventional diesel one, has been modified to preserve the electro-hydraulic driver from the high temperature through a cooling circuit. A temperature sensor was installed on the backflow line to monitor the water temperature. The injectors employed evidenced reliability issues due to the high temperatures and low-lubricating nature of the water. Different nozzle geometries have been tested. This manuscript relates to an eight-hole nozzle with a hole diameter of 0.177 mm. The performances of other nozzles are under analysis and further investigation. Three parameters of the injection system were varied for the analysis, the injection pressure (p_{rail}), energizing time (ET), and the start of the injection (SOI).

Looking at Fig. 3, the WHR system is composed of a gas-to-liquid heater and a water condenser, and it was installed on the exhaust line of the SCE. The heater using the exhaust gas as the thermal source was properly designed for 300 bar of maximum pressure, and a finned-tube configuration was used. The water condenser is a plate surface type. Table 2 displays the main geometric data for the WHR, which is also used for modelling the heat exchangers.

Table 1
Naturally aspirated SCE specifications.

Parameters	Units	Specification
Specific displacement	cc/cyl	489
Bore	mm	83
Stroke	mm	90.4
Compression Ratio	–	13.6
Valves per cylinder	–	4
NG PFI	–	Bosch NGI2
NG injection pressure	bar	8
Water direct injector	# holes x d	8x0.177

The heater was conceived to raise the water temperature by exploiting the thermal energy of the exhaust gases. It has been designed to operate with high-pressure liquid water, requiring an exhaust gas flow rate of at least ~130 kg/h and an inlet temperature of 530 °C. The condenser, shown in Fig. 4 downstream of the heater, recovers water from exhaust gases by dropping the temperature of the exhaust gases below the dew point temperature at the given pressure.

After a preliminary debug to verify the performance of the WHR system, the integration of an inductive heater, installed downstream of the exhaust heat exchanger, essentially to achieve the target temperature at lower engine load conditions and to reduce the heating transient time due to the high thermal inertia of the heater, as discussed later on. Subsequent modifications have been applied to the high-pressure water line configurations to reduce the heat transfer to the ambient through an additional insulating mat. A temperature sensor was installed close to the cylinder head and before the injector. Additional information about the inductive heating system developed for stationary application for spray analysis is reported in [24]. The condenser, shown in Fig. 4 downstream of the heater, recovers water from exhaust gases using dropping the temperature of the exhaust gases below the dew point temperature at the given pressure.

2.2. Numerical models

The complexity of the experimental setup and phenomenology under investigation makes the use of properly developed numerical models adequate for a deeper investigation and understanding of the results. Both engine and heat transfer models have been developed. Further, an additional statistical model has been employed for data post-processing. For clarity, Table 3 reports an overview of the models developed and their major outcomes.

A quasi/1 dimensional numerical model has been developed to investigate the effects of supercritical water injection on the combustion process and energy balance of the integrated engine and WHR systems (Fig. 4). All the models have been developed in the GT-ISE environment. The modelling of the engine setup has been based on the geometric dimensions and component characteristics available. The SITurb combustion model is commonly used for natural gas combustion [25] due to its high predictability. It considers the concept of flame front propagation, starting from the combustion kernel generated by the electric arc between spark electrodes. It uses a two-zone approach to track the entertainment of the mixture inside the flame, whose propagation rate depends on the laminar and turbulent flame speeds. It is worth highlighting that such a model lacks capturing the interaction effect of the water with the flame front and has been used for mass and energy balance only. The water injector is modelled with a simple model assuming the injection rate. A set of controllers was implemented, aiming to target manifold air pressure (MAP), combustion phasing (CA50) and water injector quantity as a function of the fuel flow rate.

Specific templates have been adopted for the modelling of the WHR to consider the different geometrical characteristics reported in Table 2. In particular, the “HxGeomGeneral” and “HxGeomPlate” templates have been used to model the two heat exchangers, respectively. The proposed numerical models are based on detailed structural parameters from technical drawings. Other relevant operating parameters, such as exhaust gas mass flow rate, exhaust temperature, and water coolant flow rate, have been set as boundary conditions based on the experimental data. In this preliminary assessment, the heat transfer coefficient (HTC) of the condenser, both for liquid and vapour in the single phase, was defined through the Dittus-Boelter equations. They likely overpredict

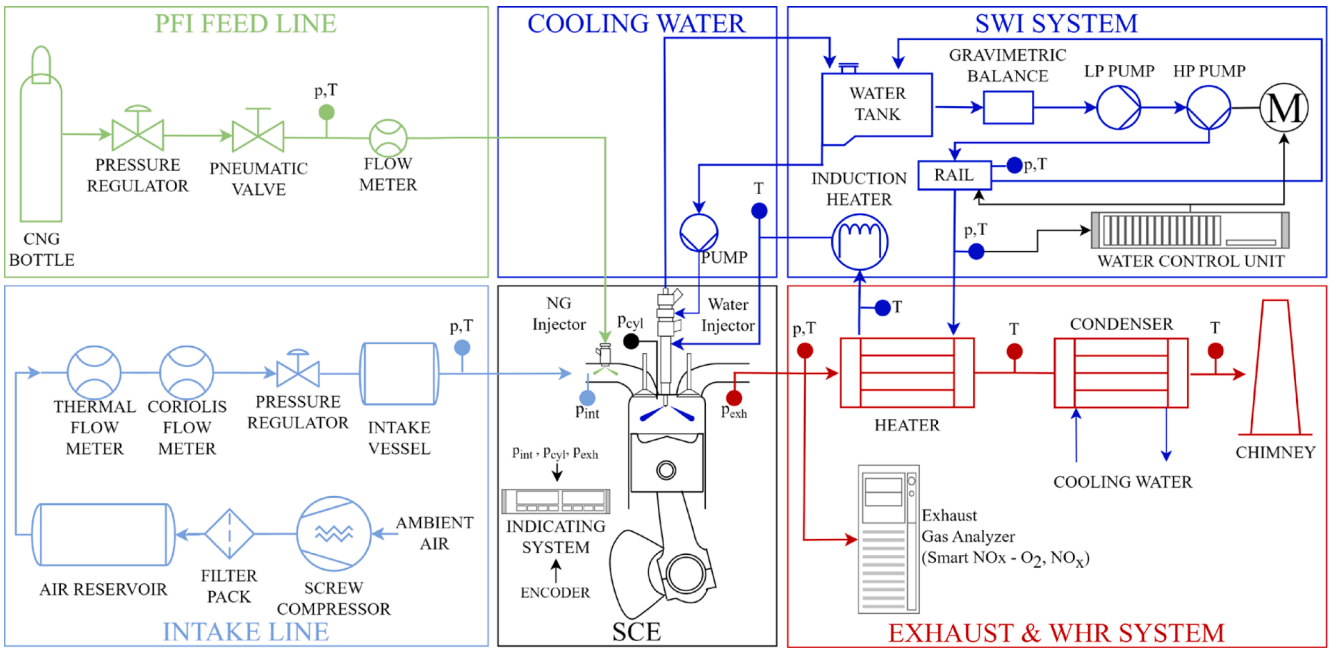

Fig. 4. Schematic diagram of the experimental setup.

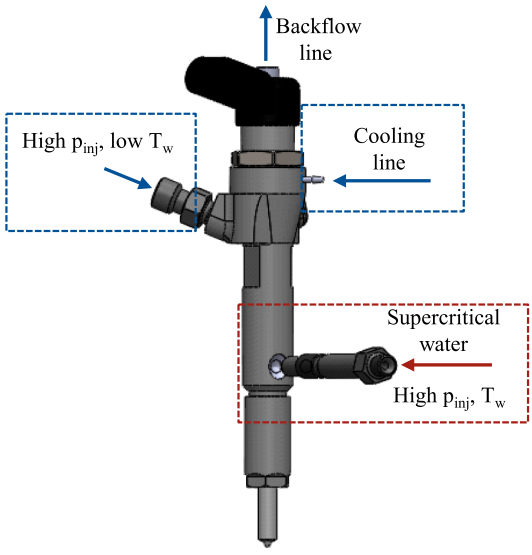

Fig. 5. A 3D render of the injector and water supply insert.

Table 2
WHR geometric parameters.

Heat exchanger	Items	Parameters	Units
Exhaust gas to water heater	Number of tubes	21	//
	Tube length	700	mm
	Tube diameter	10	mm
	Fin thickness	0.4	mm
Condenser	Plate length	710	mm
	Plate width	300	mm
	Plate numbers	21	//
	Channel height	4	mm

the real HTC in supercritical conditions [26], due to the peculiar radial temperature profile. To cope with this problem, a multidimensional approach would be needed to capture the phenomena fully [27], but this is out of the scope of this work. In the two-phase zone, when the evolving fluid condensates, the Yan et al. relation [28] was used. Similarly, for the water heater, for which the predictive Colburn correlation has been adopted, the overprediction of the HTC in the supercritical regions must be accepted as far as a multidimensional approach is used [29]. These models have been developed and integrated with the engine model to simulate the experimental setup. Their integration has required a proper technique for reducing the computational burden due to the different characteristic times of the engine and WHR system. In particular, the model has been split into two separate flow circuits, one solved with the explicit solver and the other with the implicit, aiming at reducing the real-time factor. Using two different time steps in the two circuits required a coupling between them, through a PID controller [30]. To summarize, the main model characteristics and assumptions are shown in Table 4.

The injection temperature is relevant for the analysis of the water injection effect. The temperature is not available at the injector outlet or nozzle. The thermocouple was positioned about 20 cm before the injector inlet. A proper heat transfer model for the water injection

Table 3
Overview of the developed numerical models.

Model	Method	Outcomes
WHR + Engine	0D/1D flow + combustion + heat transfer	Operating limits of WHR and water recovery capability
High p and T water line	0D/1D + heat transfer + user thermodynamical water model	Estimation of the cooling losses of the water
Injector	Statistical models (LME)	Assessment of the utility of statistical methods; Statistical validation of heat transfer model.

Table 4
The main submodels adopted.

Phenomenon	Model
Combustion	SITurb
Heat transfer	FEM for engine structures and exhaust lines
HTC	WoschniGT for the engine, Colburn for pipes, Dittus-Boelter, and
Correlations	Colburn for the heat exchanger
Turbulence	k-ε

system has been developed to address this lack of injection temperature. In particular, the model includes the final part of the high-pressure pipe and the injector (see Fig. 4). To calculate the heat transfer coefficient of the high-pressure line with the test cell environment, the Zukauskas correlation for a cylinder in a crossflow has been applied [30]. The injector model was developed based on Payri et al. diesel injector model present in the GT-Suite library [31]. The experimental water injector has been modified internally to fulfil the requirements described in the experimental setup section. The external body dimensions are unchanged, and therefore, its surface temperature and heat loss are assumed equal. A schematic of the developed model with the boundary conditions imposed is reported in Fig. 6.

It is worth highlighting that standard water models are usually applied and verified at high pressures or high temperatures, but they fail to predict the proper thermodynamical characteristics in other regions of the p-T diagram and the supercritical region. To address this issue, the International Association for the Properties of Water and Steam (IAPWS) has proposed the IAPWS-95 model, valid from the melting pressure line up to 1273 K and 1000 MPa [31]. This model assures low uncertainty (<0.1 % and 2 % for density and isobaric heat capacity, respectively) within its application domain [32]. For this study, it has been coded as user-defined functions in Fortran 90 and compiled as a library file imported into the GT-ISE environment. It has been derived from the H2OI95 Fortran code implementing the IAPWS-95 model and tailored for the specific application [33]. The validity of the coded library has been checked in the p-T domain of interest, comparing the result to both the National Institute of Standards and Technology (NIST) Chemistry WebBook [34] and the online Russian National Committee (RNT) tool of IAPWS. The model has been used to estimate the water temperature at the injector inlet and outlet (at the nozzle tip) and as a diagnostic tool. The main results are discussed in section 3.1.2.

To support the validation of this model, and as shown in the workflow chart (Fig. 3), a statistical model has been applied to the injector data to process the experimental results further and validate the heat transfer model. It is worth underlining that, advanced statistical models are helpful for better analysing complex phenomena and extensive datasets (data-driven summary). In this work, a preliminary assessment has been carried out. In particular, a linear mixed-effect (LME) model, usually applied to correlate formulas and data [35], has been adopted to describe the relationship among the injector response, the explanatory variables, and classification factors [36]. It permits identifying the explanatory variables that mostly affect the variance of the response

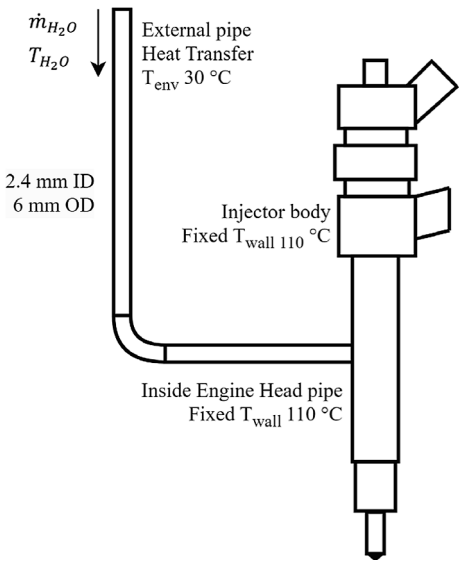

Fig. 6. Schematic diagram of the model adopted for the assessment of temperature drop at injector tip.

under analysis. The injector mass flow rate was chosen as the model response variable in the specific case. A proper procedure to define the right model formulation must be applied to get a reliable LME model. Various model formulations were built, and each model was tested and compared through performance indicators. Further details on the procedure for the model set creation are reported in APPENDIX A. The selection criterion was the lowest Akaike information criterion (AIC) value [37]. As a result, the model developed has resulted in having other than the lowest AIC, also the best Bayesian information criterion (BIC), loglikelihood, and R^2_{adj} values. This approach has allowed to validate the HT transfer model statistically and to objectively prove the low reliability of the prototype SWI designed. The results are discussed in section 3.2.3.

2.3. Test methodology

A suitable experimental testing methodology was developed to evaluate the effectiveness of the SWI concept and point out the critical issues of the prototype systems. The tests were performed in steady-state operating conditions at fixed engine speed and varying the engine load. It involved partial and full load operations at 1500 and 2000 rpm in stochiometric conditions. The tests have been carried out by varying the CA50 (Table 5), to obtain a NG baseline for further comparison of the direct water injection effect. The experimental results were also used to validate the numerical engine model developed and described in Section 2.2.

Based on the NG baseline, the SWI concept assessment was performed at part load conditions at different engine speeds, specifically 1500 and 2000 rpm at 600 mbar of MAP. The NG calibration settings were adopted, at constant Spark Advance (SA) and lambda values. A parameterization study was conducted to evaluate the impact of direct water injection on the combustion process, cycle efficiency, and emissions. Two injection parameters, water/fuel ratio (W/F) and Start of Injection (SOIw), have been considered. The SOIw has been varied to evaluate the injection timing threshold at which the water injection spray tends to quench the flame front. Different W/F levels that are compatible with the operating point and heating potential of the W/F system have been explored. The SOIw variation was performed for all W/F levels at 1500x600 and 2000x600. Table 6 provides an overview of the sensitivity activity.

It is worth highlighting that the thermodynamic characteristics of water in the supercritical region show a strong nonlinearity. In fact, in the region of the critical temperature and a narrow interval around the critical pressure (221 bar), the thermodynamic properties are highly sensitive to the temperature, as observed for isobaric specific heat capacity (c_p) and density (ρ) in Fig. 7. In particular, the peaks of c_p, increases up to supercritical pressure and then decrease as the pressure rises and the differences in thermophysical properties become less noticeable. The non-linear trend of water properties strongly influences the heat transfer process under critical conditions. A p_{rail} of 300 bar permits to achieve higher densities and temperatures at the same thermal energy supplied. Such thermodynamic conditions should permit, during the fluid injection into the combustion chamber, to avoid having the bi-phasic state, which could cool the in-cylinder mixture. For control

Table 5
Test matrix for NG baseline.

[Engine speed]x[MAP] *[rpm]x[mbarA]*		CA50 *[deg aTDC]*					λ *[-]*	SOI_{NG} *[deg aTDC]*
1500	600	4	8	12	14	16	1	−360
	800							
	1000							
2000	600							
	800							
	1000							

Table 6
Test matrix for supercritical water concept assessment.

Test point [rpm]x[mbarA]	SA [deg aTDC]	λ [-]	SOI_{PFI} [deg aTDC]	SOIw [deg aTDC]						p_{rail} [bar]	W/F [-]
1500x600	−11	1	−360	−5.5	−1	3.5	–	–	–	300	0.3
				−5.5	−1	3.5	6.5	–	–		0.4
				−5.5	−1	3.5	–	–	–		0.8
				−5.5	−1	3.5	6.5	–	–		1.4
2000x600	−19			−5.5	–	–	6.5	12.5	18.5		0.3
				−5.5	−1	–	6.5	12.5	18.5		1
				−5.5	−1	–	6.5	12.5	18.5		1.8

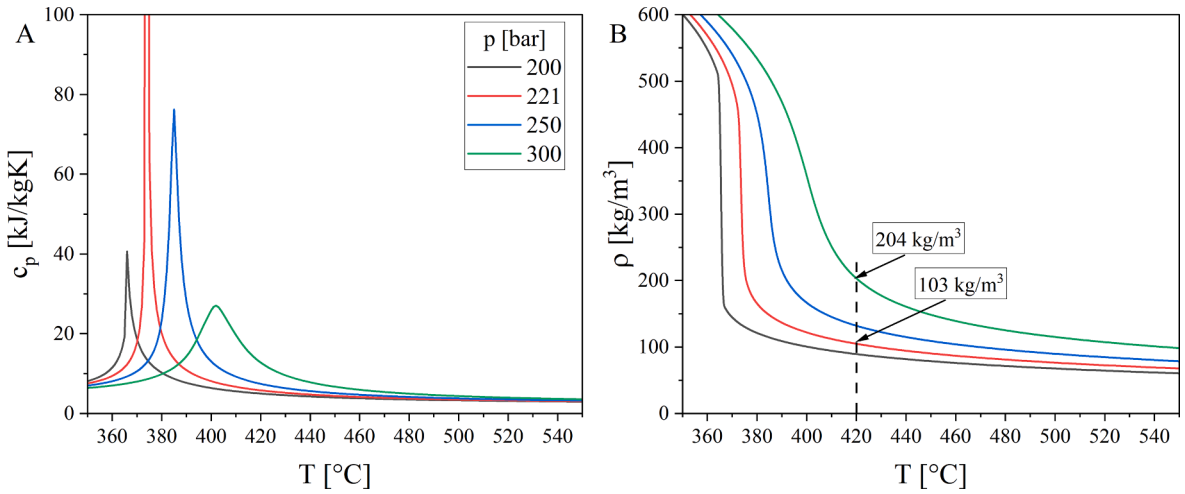

Fig. 7. C_p (A) and ρ (B) vs. temperature diagrams of water at different pressures [38].

and numerical purposes, the target temperature was measured as close as possible to the injector and the engine head and after the inductive heater.

An efficiency evaluation of the WHR system integrated into the SCE application is proposed through the experimental and numerical model in Section 3.1.1.

3. Results and discussions

3.1. Numerical analysis

This section presents the main numerical results obtained using the models developed in section 2.2. The SCE and WHR integrated model has been used for the performance assessment of the system, and the water injector system model has been used to estimate heat loss.

3.1.1. SCE-WHR integrated model

The developed SCE-WHR model has been tuned using the experimental data at two engine speeds, different loads, and spark timings (see Table 5) through an optimization procedure by means of a genetic algorithm. All the experimental data are relative to the operation of the engine with NG only. For example, in Fig. 8 the pressure traces obtained by the numerical model are compared to the experimental data. The shaded bands consider the cycle-to-cycle variability on 256 consecutive measured pressure cycles. The traces confirm the satisfactory results of the predictive combustion model to the variation of the chosen variables.

Fig. 9 reports a comparison between experimental and numerical results. The other engine boundaries, such as iMEP, combustion duration and timings, air and fuel mass flow rate, and peak pressure and position, are correctly captured. Scatter bands of ± 5 % and ± 10 % are

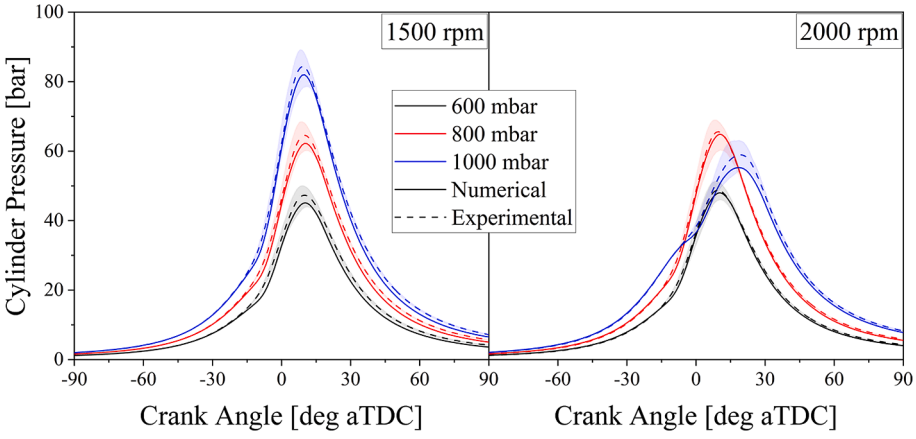

Fig. 8. Experimental-numerical comparison of the in-cylinder pressure traces for 6 operating points varying speed and load.

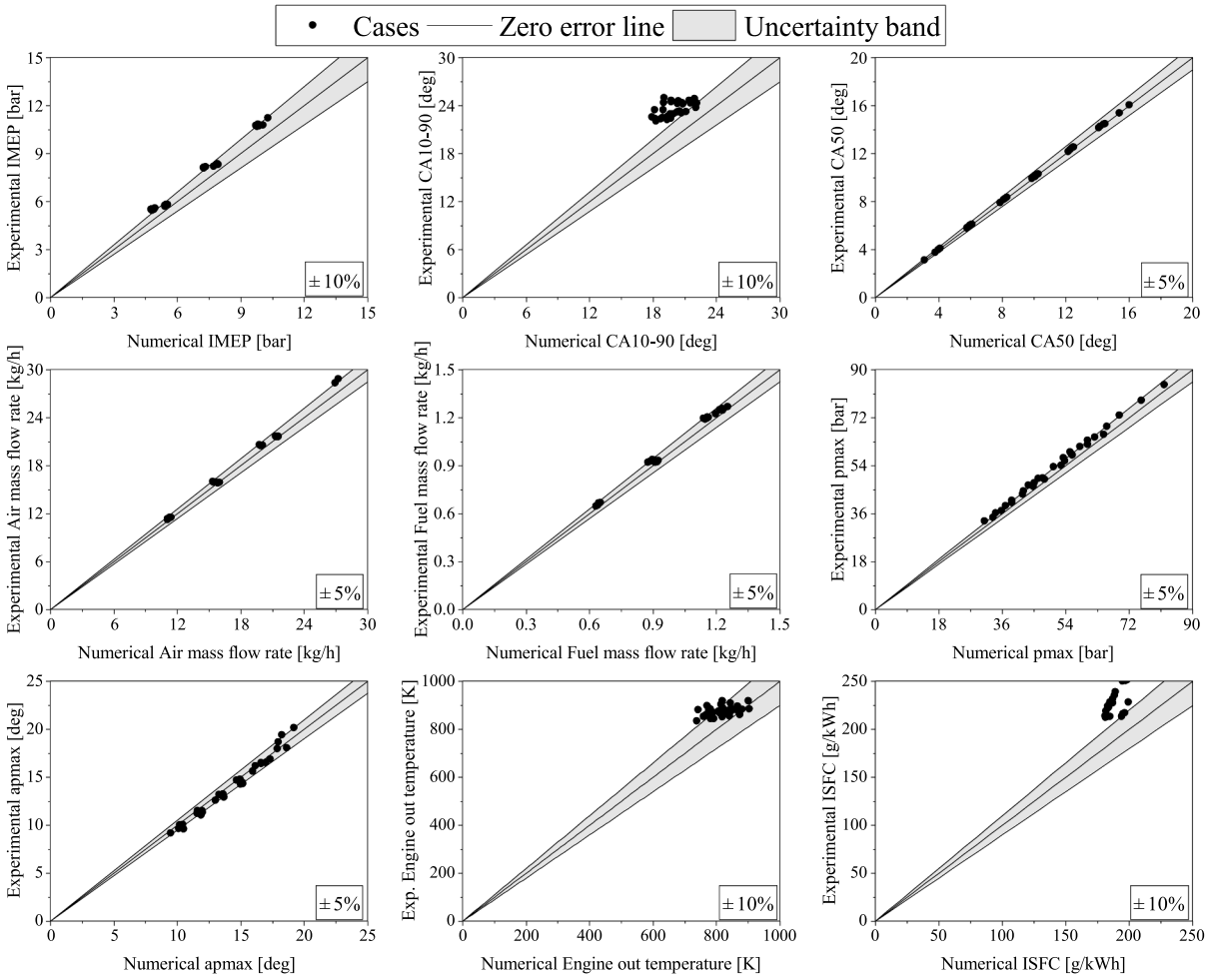

Fig. 9. Experimental-numerical comparison of engine and combustion data with uncertainties bands.

included. Some outputs, such as the indicated specific fuel consumption (iSFC), are affected by the propagation of other errors (iMEP and fuel consumption), resulting in wider scatter bands. However, the results show that exhaust mass flow rate and temperature prediction are acceptable.

Regarding the WHR, the highly transient nature of the system and the dependence on several parameters make the predictivity of its model challenging. First, in the warm-up phase of the water injection system, the water was injected continuously avoiding local high-temperature zones and promoting uniform temperature distribution among the components. However, continuous operation (for hours) has shown some issues with the various injectors used due to the low lubrication characteristics of water, impacting mainly on repeatability over time. Thus, the high thermal inertia of the WHR system has posed some limits to operations in reaching stationary operating conditions. This is confirmed by the numerical model, which requires about 2 h to reach the steady state. Indeed, the numerical trace plotted against the experimental points of two different test days validate the model (Fig. 10). The numerical temperature trace matches the time evolution of the experimental results. Uncertainty has been added to the experimental results to consider differences in temperature measurement point, water flow rate variation, and engine combustion timing between the experimental setup and numerical model.

Then, the model was used to assess the operation of the system on engine operating points not explored experimentally because of the issues related to the complex water injection system for high heated water flow rates. The speed has been varied from 1000 to 4000 rpm and the load from 0 up to 100 %. The main research question aims to determine

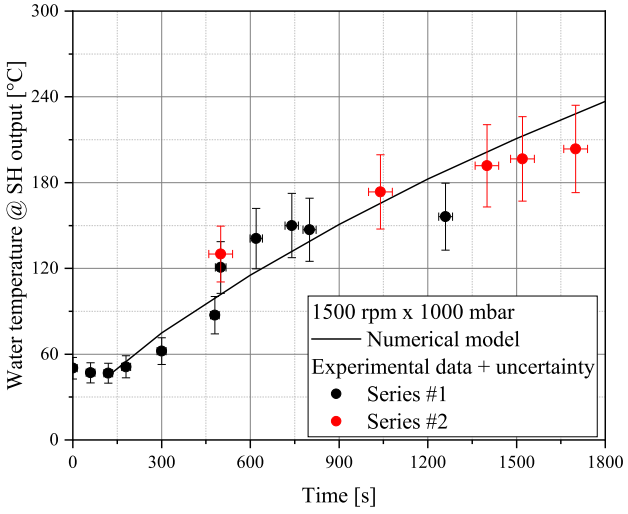

Fig. 10. Experimental-numerical comparison of temperature–time traces for WHR model validation.

the engine operating regions where the available heat recovered from the exhaust gases can bring the water to the supercritical state through the WHR. Fig. 11A) reports the *iso*-W/F water regions at supercritical conditions, as a function of the engine speed and load, exploiting the exhaust thermal power shown in panel B). At low engine speed (<1500

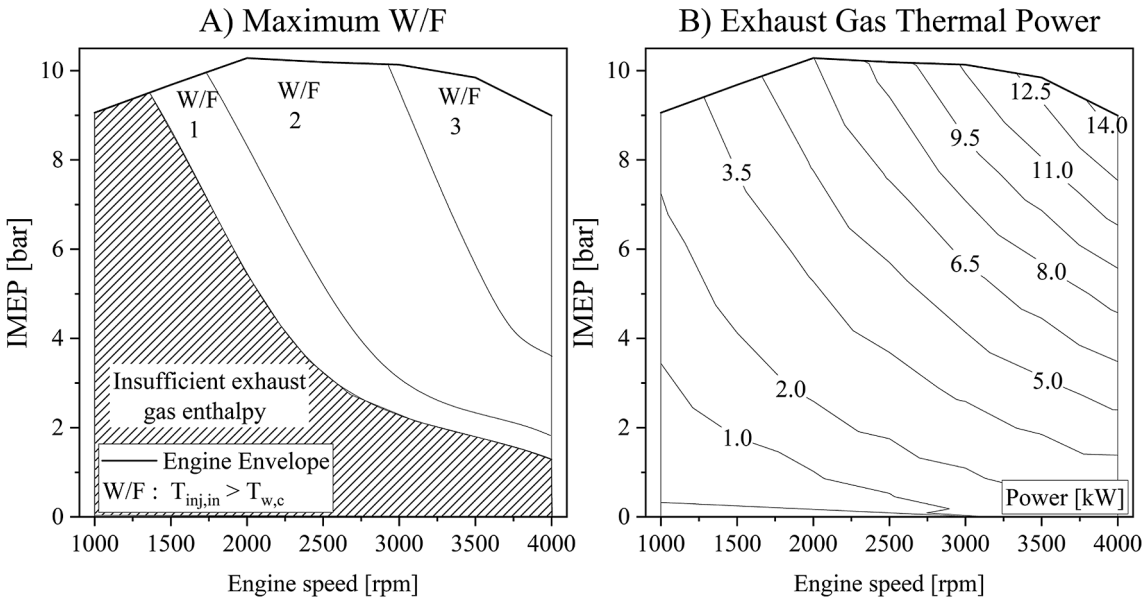

Fig. 11. WHR performance as maximum W/F compatible with supercritical condition (A) and exhaust gas thermal power (B).

rpm) the lower thermal power content of the exhaust gas does not permit achieving the supercritical temperatures when using W/F values above 0.5. W/F of 3 can be achieved only from 3000 rpm and near full load conditions to 4000 rpm at medium–high load conditions. W/F below 2 can be achieved in a wider operating range. It is important to underline again that, the critical water temperature at the exit of the heater was reached after a long transient period, ranging between 2000 and 6000 s.

The condenser design and its characteristics have turned out to be capable of recovering almost all the water deriving from combustion over the whole engine operating map. On the other hand, the heater has resulted in low efficiency at lower load conditions.

3.1.2. *Injection system HT model*

The heat transfer model of the high-pressure line was developed to investigate the undesired cooling process of water further. The results show that it is not sufficient to maintain those conditions at the injector outlet once it reaches the supercritical conditions downstream of the additional inductive heater. The simulated results are plotted in Fig. 12, which compares the temperature at the injector inlet and outlet. The non-linear variations of water properties such as density, thermal conductivity, Prandtl number and viscosity with pressure and temperature produce a non-monotonic trend in heat transfer rate with mass flow rate. The simulated temperature drop between the heater and the injector inlet is about 120 °C, with an additional 100 °C drop inside the injector. Consequently, the calculated injection temperature is about 220 °C, below the desired supercritical conditions. The water at the injector nozzle exit (300 bar, 220 °C) lies in the compressed fluid region being in a liquid phase. The fluid density and specific enthalpy in this operating point are 860 kg/m3 and 0.95 MJ/kg in comparison to the values at the supercritical target points of 360 kg/m3 and 2.15 MJ/kg (see Fig. 1).

The primary concern regards the reduction of the losses through a proper insulation system. Crossing the results of the engine operating map with the heat transfer model, it is possible to estimate the mass flow rate and the heater requirements to ensure supercritical conditions. Achieving the supercritical conditions at the injector inlet requires a flow rate higher than 4 kg/h and a temperature higher than 650 °C. These values rise to 9 kg/h and 900 °C to achieve the supercritical conditions at the injector outlet. These values could be affected by a certain degree of uncertainty related to the boundary conditions

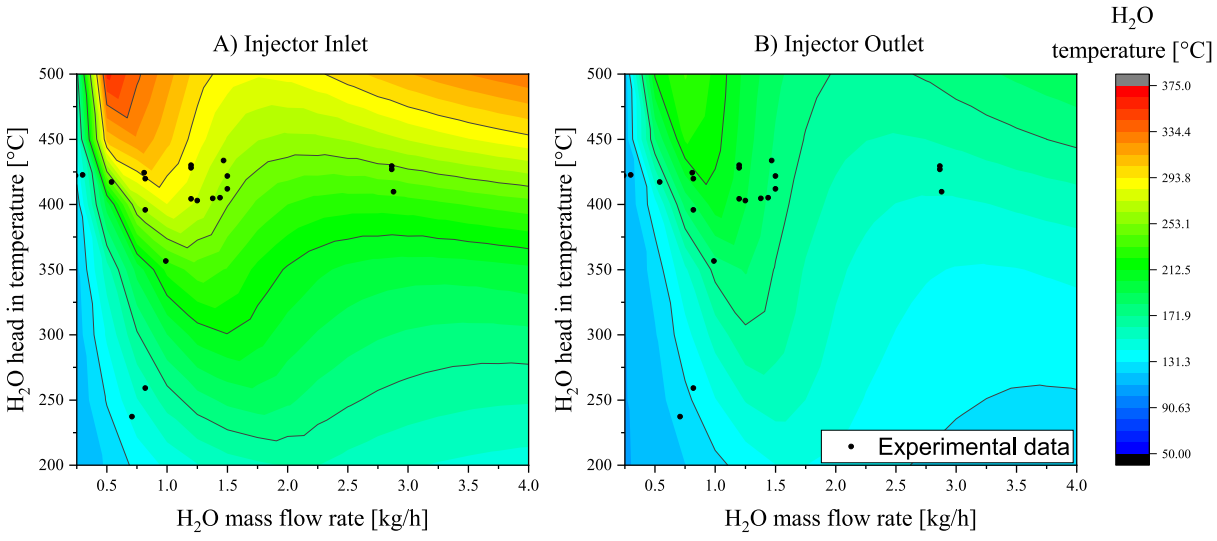

Fig. 12. Simulated water temperature as a function of mass flow rate and temperature. a) temperature at injector inlet a) and outlet b).

imposed, such as the injector body temperature, ambient temperature around the cylinder head and injector body, etc. As a result, improvements to the SWI system are required in terms of insulation, injector design, etc.

3.2. Experimental analysis

This section presents the experimental analysis of the effect of direct water injection at high temperatures on the combustion process, NOx emissions, and energy balance. Sections 3.2.1 and 3.2.2 discuss the results of the experimental campaign, specifically designed to assess the influence of W/F and SOIw parameters on the combustion process while examining the spray-flame interaction. An assessment of the pros and drawbacks of the prototype system is also presented. Section 3.2.3 presents the statistical analysis to assess the intrinsic difficulties in the experimental setup and validate the heat transfer model. Finally, section 3.2.4 discusses the overall energy balance of the integrated system.

3.2.1. W/F effect

A parametric analysis has been performed to evaluate the effect of the direct water injection on the combustion process. Moreover, the heating system performance has been analysed regarding the injection temperature and the phase state of the water. Fig. 13 shows the water temperature for different water mass flow rates during the test campaign.

As shown in Fig. 13, the temperature decreases as the water flow rate increases, with a reduction of about ~40 °C passing from 0.24 kg/h to 1.4 kg/h. Due to variations in temperature as a function of water flow, the range was limited up to 1.4 kg/h to minimize differences. Furthermore, as emerged from the numerical analysis, a considerably lower injection temperature is expected in correspondence to the injector nozzle. A temperature drop up to 200 °C for the explored conditions has been calculated. Further information can be found in the previous section "Injection system HT model". Based on this consideration, Fig. 14 displays the different water phases in the pressure-specific volume diagram with the states reached in correspondence to the injector nozzle (Tw nozzle) and reached in the inductive heater (Tw heater). This diagram aims to define the state of water in the nozzle before injection based on the cooling effect evaluated through a numerical model. Despite reaching the supercritical state within the heating system, it did not achieve the supercritical conditions at the injector out. However, the following section evaluates the effect of water direct injection in subcritical conditions in a liquid state.

Thus, the analysis focuses on the impact of high-temperature direct

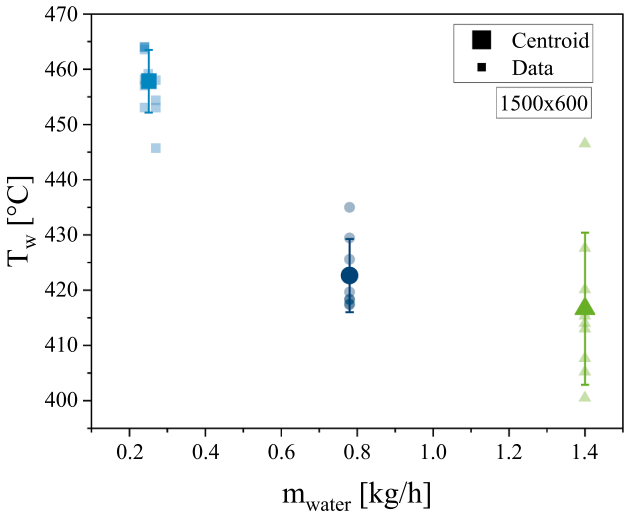

Fig. 13. Water temperature function of the mass flow rate.

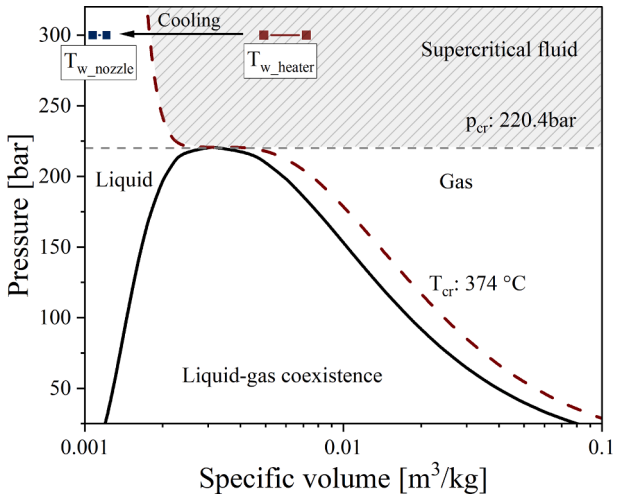

Fig. 14. p-v diagram of water [38].

water injection in subcritical conditions on the combustion process. The in-cylinder pressure (Pcyl), rate of heat release (HRR), heat release (HR) and water injector signal for different W/F levels are displayed in Fig. 15. The results refer to the test point at 1500 rpm, MAP 600 mbarA, SA −11 deg aTDC and lambda 1. NG case has been included for the evaluation of the direct water injection effect. The numerical model estimated a water injection temperature of approximately 250 °C for these tests.

The water injection determines the cooling effect of the combustion chamber, proportional to the W/F level. It significantly affects the charge compression stage and the consequent combustion process, as shown in Fig. 15. This aspect was also highlighted by Zhao R et al. [39], as by injecting during the compression stroke near TDC, the in-cylinder temperature becomes higher than the water. Therefore, the water absorbs heat from the air, thus reducing the temperature in the combustion chamber, resulting in a lower peak pressure. The injected water requires more energy to vaporize, proportional to the W/F, resulting in a slower combustion reaction rate and lower in-cylinder temperatures. In the case of lower W/F ratios (0.3 and 0.4), for which the cooling effect is not significantly evident, there is an increase in the HRR peak and the peak firing pressure. There is an increase in the flame propagation rate, as demonstrated by the higher HR rising edge in the angular interval 20–30 deg. This effect is likely due to the water jet flame front interaction. CFD analysis has shown that varying the injection parameters positively affects the flame propagation speed, which can be achieved by balancing jet momentum and turbulent kinetic energy effects [40]. Similar trends are also observed at 2000 rpm, as displayed in Fig. 16. In this case, the injection timing is imposed at SOIw −5.5 deg aTDC, p_{rail} of 260 bar, and SA, keeping constant at −19 deg aTDC for all test cases. Similarly to the 1500x600 operating point, for the lower W/F case (0.3), a slight slowdown can first be noticed after the water injection and then a speedup of the combustion process, resulting in higher cycle work.

Fig. 15 and Fig. 16, show that the increase of the W/F, above values of about 0.4, results in a significant decrease in the maximum HRR and PCYL for both test points. In particular, this effect starts before the water injection, which indicates a cycle-to-cycle dependency. A possible explanation is that the increased injected water led to a rise in the internal EGR. Proof of this hypothesis is given by the reduction of about 3 % of the air flow rate, as reported in Fig. 17. Overall, no substantial effects were observed at lower W/F ratios.

Fig. 18 displays the iMEP, CoVimep, Pmax and APmax results for both engine speeds. For reduced W/F ratios, there is a slight increase in iMEP of about 0.1–0.2 bar for both test points. As the W/F ratio increases, charge cooling losses and possible flame water jet interaction, lead to penalties in terms of iMEP and CoVimep, worsening the

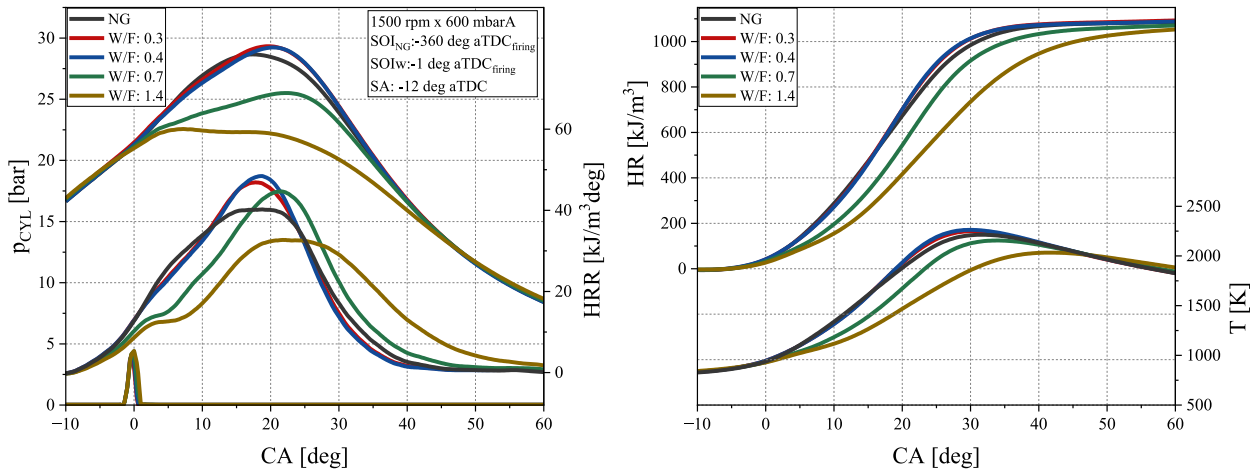

Fig. 15. In-cylinder pressure, HR and HRR at different W/F levels, compared to the NG reference case at 1500 rpm and 600 mbarA.

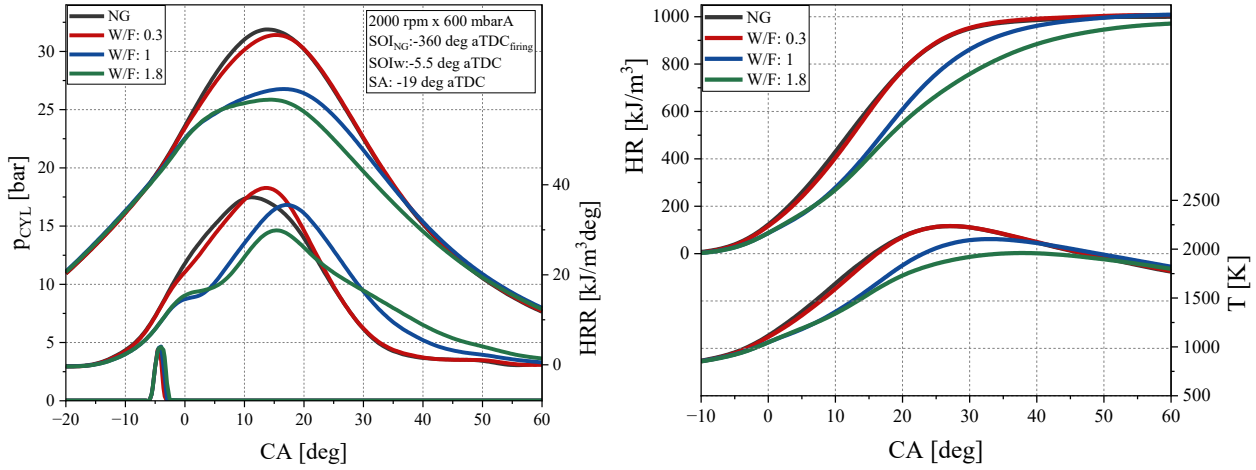

Fig. 16. In-cylinder pressure and HRR sensitivity at different W/F at 2000 rpm and 600 mbarA.

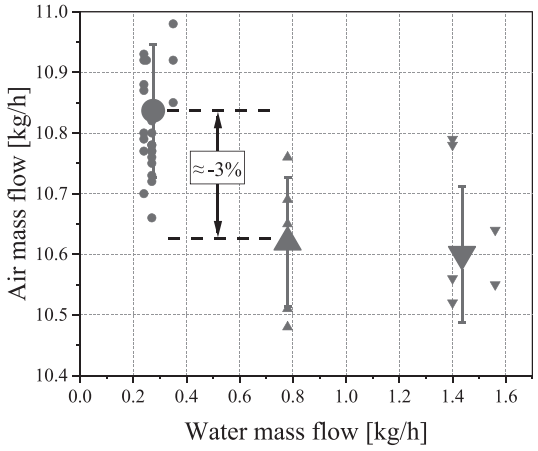

Fig. 17. Effect of water mass flow on air mass flow at 1500x600.

combustion process with values up to 5 %. At low engine speed, the water injection also causes a slight increase in the Pmax, contributing to the greater working cycle for reduced W/F levels. This trend is not evident at 2000 rpm. In fact, the direct water injection causes a slight reduction of the Pmax and a delay of the APmax, mainly due to the worsening of the flame propagation speed at the initial stage of the combustion process. At the highest W/F, a reduction of the Pmax of about 6 bar is observed for both test points.

To provide a more detailed analysis of the effect of direct water injection on the combustion process, Fig. 19 displays the combustion duration values, including CA0-10, CA10-50, and CA50-90 for the 1500 rpm. With an injection timing of −1 deg aTDC, the water injection for reduced W/F values affects CA90. Specifically for the W/F 0.4 case, it reduces CA50-90 by 1.2 deg due to the increased flame front propagation. An increase of W/F results in a higher SA-CA10 due to a greater cooling effect, leading to a delayed CA50 and prolonged combustion duration (CA10-90). These results demonstrate that the direct injection of water at high temperatures significantly impacts the combustion process. In particular, the W/F parameter is crucial in increasing flame front propagation rate and improving air–fuel mixing.

The direct water injection reduces NOx emissions while maintaining IMEP values. At 1500 and 2000 rpm, there is a proportional reduction in NOx with a W/F increase. The water injection strategies lead to a significant impact of water spray on the flame front, which results in a substantial reduction in NOx formation. The numerical simulation demonstrated that the local decrease of in-cylinder temperature and increased gas-specific heat near the flame front inhibited NOx formation [41]. Arabaci also obtained similar results through an experimental activity on a six-stroke engine with a reduction of NO up to 50 % [42]. For the best case, W/F 0.3 at 2000 rpm, a reduction of 53 % is observed compared to the NG case. As water consumption increases, it leads to more heat absorption, which further decreases NOx concerning the

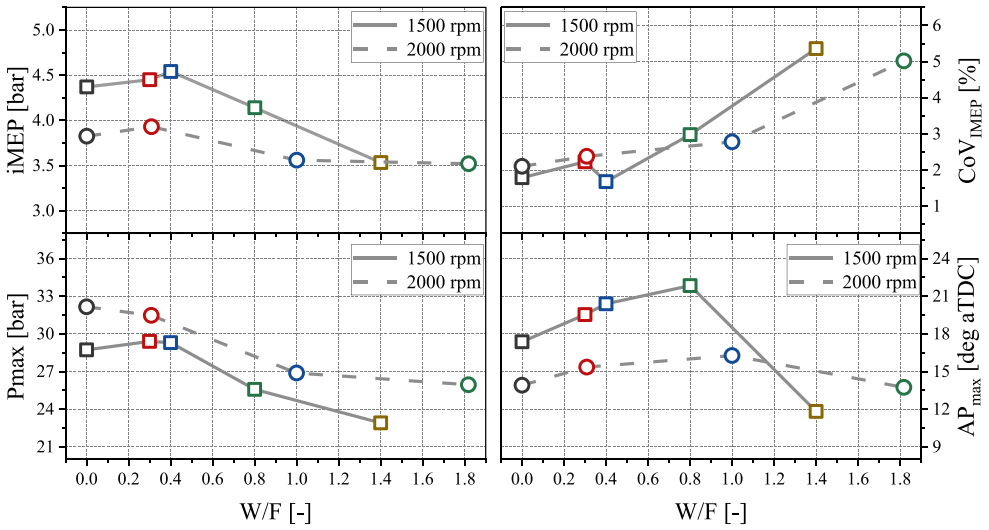

Fig. 18. Effect of W/F on iMEP, CoV_{IMEP}, Pmax and APmax for all test cases.

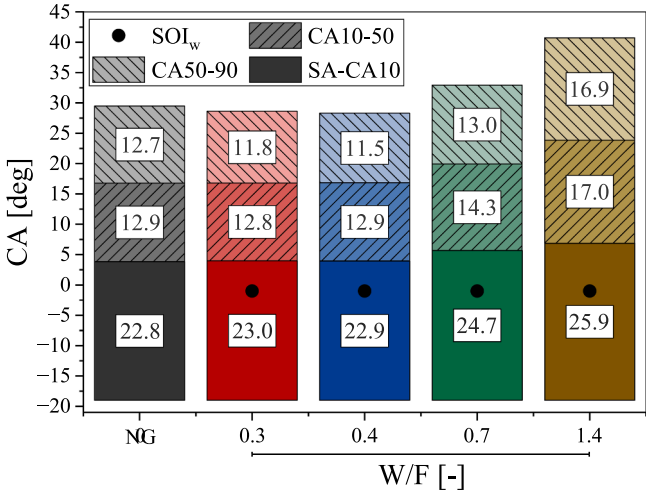

Fig. 19. W/F effect on CA0-10, CA10-50 and CA50-90 at 1500x600 and SOIw −1 deg aTDC.

natural gas reference case. In extreme cases, the NOx reduction effect is mainly due to the deterioration of the combustion process (see the high COVimep values).

The energy balance completes the analysis of the performance of the integrated system. Fig. 21 displays the energy balance results of the integrated system for three operating points, at 1500 rpm and 2000 rpm, for different W/F levels. It should be considered that the WHR is designed for higher exhaust gas flow rates, resulting in significantly lower performance. In Fig. 21 a) and b), it is observed that direct water injection with W/F levels of 0.3–0.4 improves the brake power by about 0.11–0.12 kW. Looking at cases reported, about 1 % higher brake efficiency can be achieved. The estimated direct water injection (DWI) efficiency evaluated according to the following formula is about 5 %, similar to other WHR solutions such as TEG.

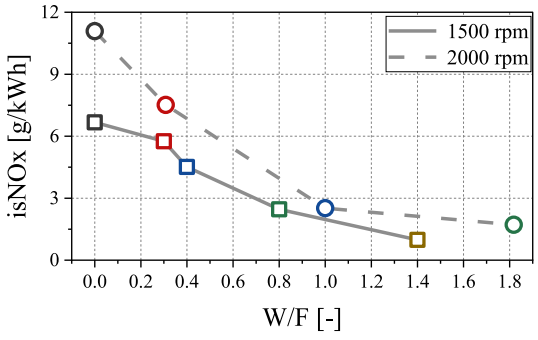

Fig. 20. W/F effect on NOx.

$$\eta_{DWI} = \frac{\Delta P_{brake}}{Q_{exh}} \quad (1)$$

Where ΔP_{brake} is the engine brake power difference between the NG and DWI operations. Q_{exh} is the thermal power of the exhaust gases.

3.2.2. *Water injection timing effect*

The injection timing sensitivity has been analysed to evaluate spray-flame front interaction. For the sake of investigation, only the 1500x600 test case has been considered for the comparison since the results are similar to those detected in the other operating points. Specifically, three different SOIw values at constant W/F = 0.4 are reported in Fig. 22. The NG reference point is added to provide a valuable comparison of the iteration process.

A significant influence of the SOIw on the combustion process is observed in the combustion evolution process. For an SOIw near the TDC, the spray is close to the flame front, determining a significant effect on the heat release rate. For the cases at SOIw −1 and 3.5 deg, an increase of Pmax is observed up to 29.5 bar, with a slight difference in terms of iMEP, comparable to the CoVimep. As the delay increases, this effect disappears. Fig. 23 analyzes the impact of the injection timings on combustion phasing.

A significant influence occurs for injection timings close to the TDC, especially on the CA90. The maximum reduction occurs in advancing the SOIw values. This analysis demonstrates that SOIw and W/F are significant parameters affecting the evolution of the combustion process. As for the W/F sensitivity, the SOIw impact on NOx emissions has also been analysed and presented in Fig. 24. Injection timing close to the TDC significantly affects the NOx formation mechanism, as the water mitigates the local in-cylinder temperature and increases the gas-specific heat. The maximum benefit is obtained with W/F = 0.4 and SOIw = -1 deg, with a NOx reduction of approximately 30 % compared to the NG reference case.

In general, water injection not at supercritical conditions, as demonstrated through an analytical approach discussed in the “Injection system HT model” section, significantly affects the combustion process. In particular, these preliminary analyses allowed us to evaluate the

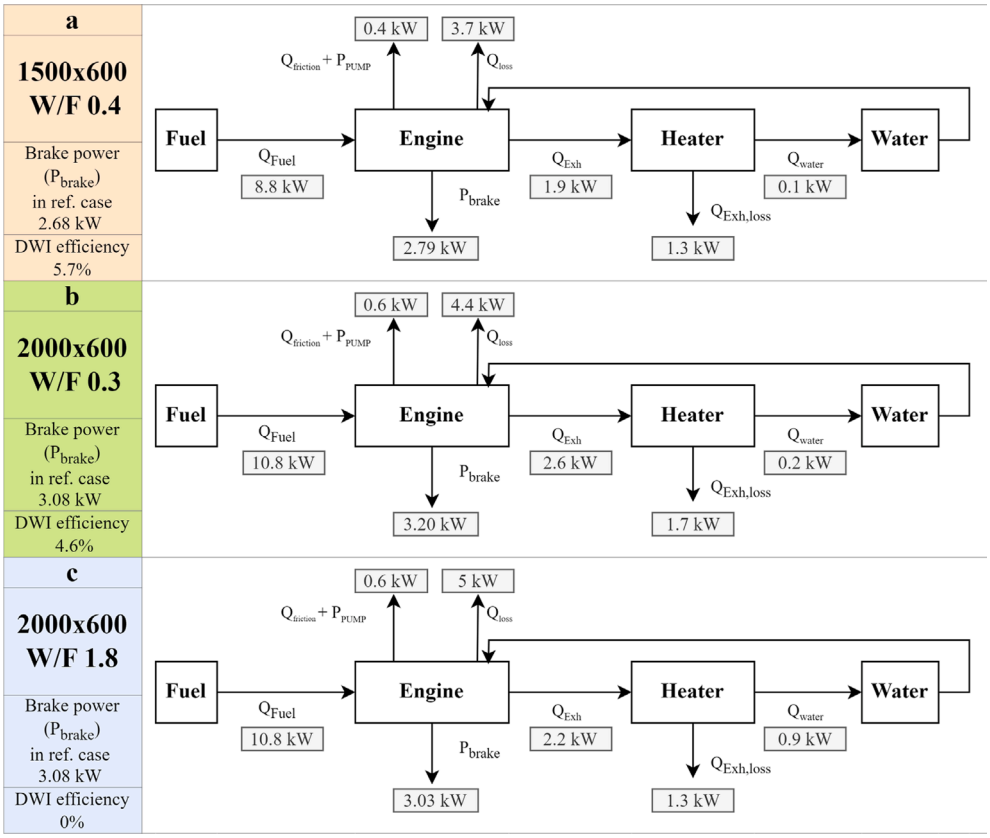

Fig. 21. Energy breakdown of the engine and WHR system. a) 1500x600; b) 2000x600; c) 2000x600.

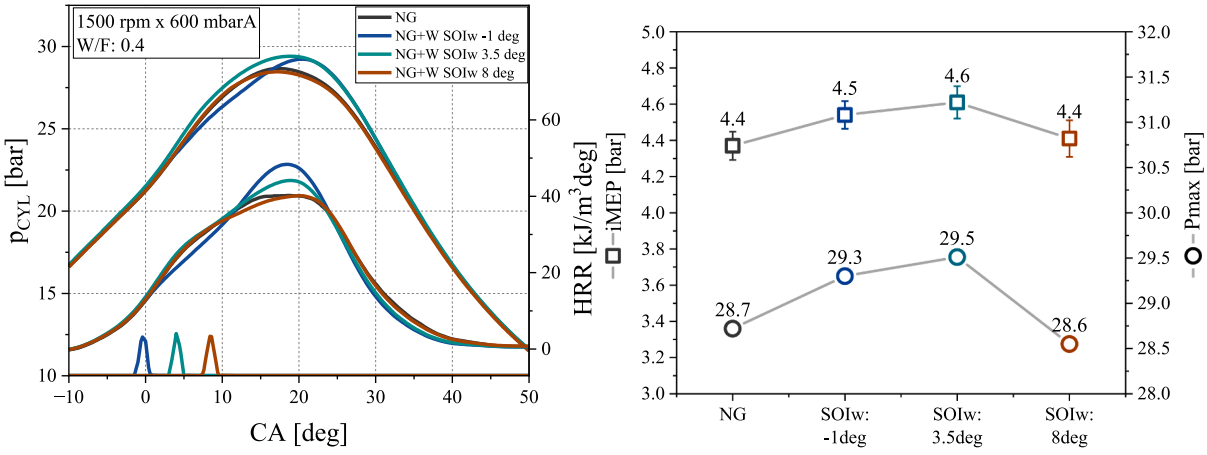

Fig. 22. In-cylinder pressure and HRR sensitivity at different SOIw cases at 1500 rpm and 600 mbarA (top). Effect of W/F on iMEP and Pmax (bottom).

effect of water on the combustion process and how injection parameters influence it. W/F values of 0.3–0.4 and injection timing close to the TDC ensure the best performance for the ranges explored, both in terms of thermodynamic cycle and NOx. The analysis shows that although improvement can be achieved through DWI, it is not obvious due to the complex interaction between combustion and water injection timings and evolution. Indeed, for many operating parameter settings, there is a worsening of engine brake efficiency.

3.2.3. *Statistical modelling and future outlook*

The experimental assessment of the SWI concept through a WHR system has required a huge effort to develop the prototypal systems and experimental campaign. During the test campaign, problems arose, with the main concerns about the injector durability due to thermo-mechanical stress and low lubricant properties of water. Indeed, the tight tolerances of the injector nozzle have caused needle seizing, and during the testing campaign, it was necessary to replace nozzles due to irreversible damage. As already argued in the methodology section, different nozzles were tested. The numerosity of the data and the complexity of the phenomena involved have required additional numerical and experimental diagnostic work. In this regard, statistical methods effectively supported the experimental data analysis, providing valuable insights.

In the following, the results of a statistical method are reported and applied to the experimental data. Further, the method has been used for the validation of the injector heat transfer model discussed in section

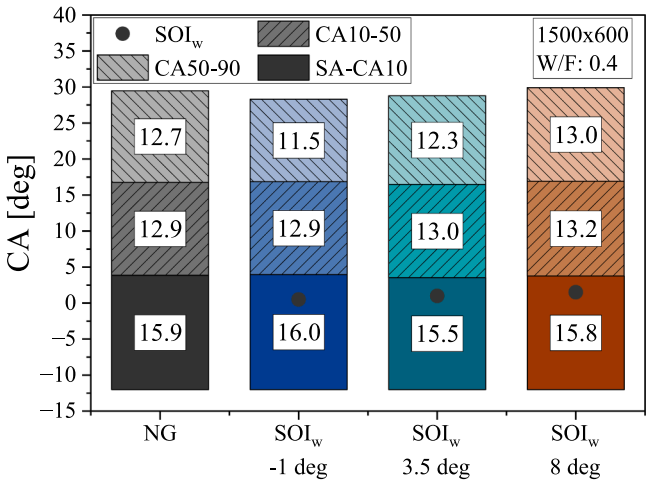

Fig. 23. SOIw effect on CA0-10, CA10-50 and CA50-90 at 1500x600 and W/F = 0.4.

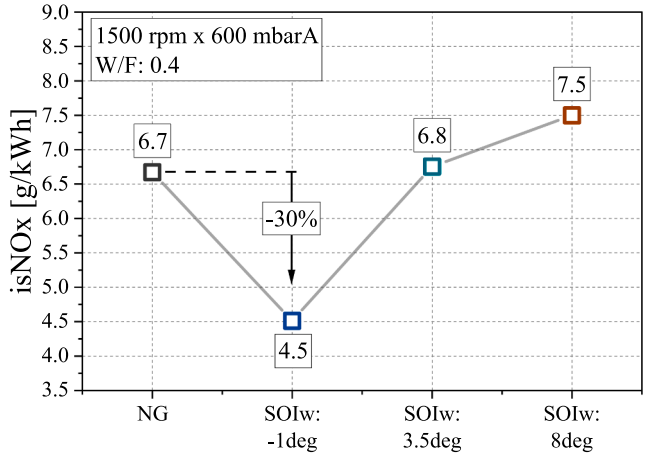

Fig. 24. Effect of SOIw on isNOx at 1500x600.

3.1.2. In particular, the LME model described in section 2.2 has been adopted to process the experimental data of the SWI system allowing to define the best model formulation (more details can be found in APPENDIX A). The results of the best model referred to as the mass flow rate, are reported in Fig. 25. A R^2_{adj} value of about 0.83 is achieved providing, an acceptable predictivity of the explanatory variables.

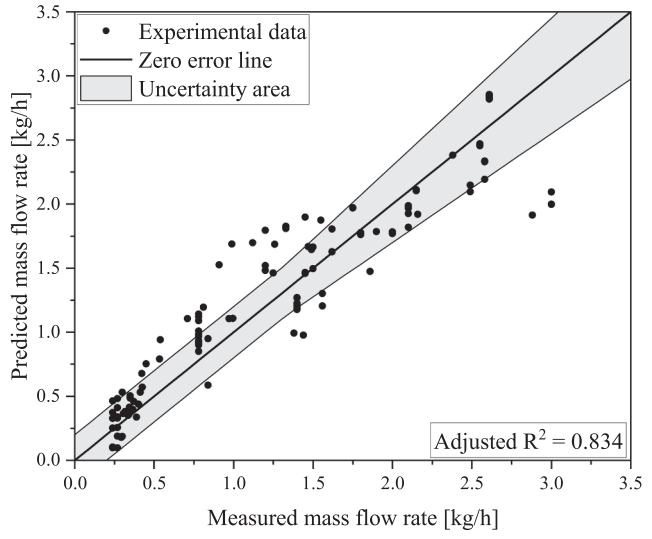

Fig. 25. LME injector model tested with experimental data.

The best-suited model formulation is reported in the following using the Wilkinson notation:

$$m\ 1 + ET + T_{inj,in} + p^{*}ET + (1|ExperimentalSetup) + (1|OP) \quad (2)$$

Where *ET* is the injector energizing time, $T_{inj,in}$ is the injector inlet temperature predicted by the heat transfer model, *p* is the injection pressure. *ExperimentalSetup* and *OP* are categorical variables, defining the particular experimental test bench configuration and the operating point respectively. As a result, the *ExperimentalSetup* variable resulted as one of the most influential factors, also confirmed by testing the model by excluding the variable (Table 8, APPENDIX B). This result confirms the complexity of the experimental system, especially the low repeatability of the injector, due to various subfactors including nozzle changes, injector body disassembly and assembly, etc..

The statistical methods can also be employed for model validation when classical comparison and performance indexes cannot be applied. This is the case for the developed HT injector model, for which fundamental experimental data, to validate the model, are not available. A temperature sensitivity analysis of the model (equation (2) has been carried out by exchanging the $T_{inj,in}$ with T_{exp}, and $T_{inj,out.}$ variables representatives of the experimental and predicted nozzle temperatures, respectively, maintaining constant the others. The assessment of the three model formulations is reported in Table 9 of APPENDIX B. The significance of the result has been analysed through a hypothesis test, particularly the null hypothesis, to evaluate whether the considered parameters influence the response variable. To this end, ap-threshold of 0.05 was adopted. Model results with p-values below this threshold mean that the parameters under evaluation through the model are statistically significant in terms of response variables. In this case, the impact of the parameter T_{exp} is not statistically significant ($p \approx 0.97$) on the mass flow rate, in comparison to the other parameters of the model. On the other hand, the significance of $T_{inj,in}$ ($p \approx$ 1e-12), and $T_{inj,out}$ ($p \approx$ 7e-9) can be interpreted as a validation of the heat transfer model. Additionally, the higher R^2 values obtaining the numerical temperatures (Table 9 of APPENDIX B) confirm the validity of the HT model and of the proposed approach.

4. Conclusions

An engine and waste heat recovery systems have been developed and integrated to assess the supercritical direct water injection concept as a possible solution to recover the wasted exhaust heat of the engine. In particular, the prototype systems integration has been analysed in detail, highlighting the benefits and limitations that emerged from the experimental and numerical activities. The main outcomes of the study are listed below.

- Both an experimental and numerical diagnostic tool have been developed to prove the impact of direct water in supercritical conditions. The recovery limits have been assessed at supercritical conditions.
- The numerical model has estimated the heat loss through the high-pressure pipe and the water injector. The heat loss causes a temperature drop of up to 200 °C, limiting the SWI application in the current configuration. Reduction of the heat losses through the system is mandatory, in particular in the injector body.
- The SWI was not reached, therefore the effect of direct injection of water at high temperatures was analysed. The injection timing and the W/F play a significant role in the combustion process evolution. Reduced W/F and SOIw close to the TDC represent the optimal injection strategy for the range explored. It determines an enhancement of the combustion speed without causing significant mixture

cooling. An increase of about 1 % in brake efficiency can be achieved with direct injection of water.
- The direct water injection significantly reduces NOx emissions and directly depends on the W/F level. The maximum reduction (-30 %) is obtained with W/F 0.4 and SOIw −1 deg, without penalties of iMEP.
- A statistical analysis using LME models has been demonstrated to be a valuable diagnostic tool for further analysis and confirms the issues faced with the experimental activities in applying the SWI concept.

Future activities will be oriented to improve the experimental system facing the issues encountered in applying the SWI concept.

CRediT authorship contribution statement

Roberto Ianniello: Writing – review & editing, Writing – original draft, Investigation, Formal analysis, Data curation. **Michele Pipicelli:** Writing – review & editing, Writing – original draft, Investigation, Data curation. **Giuseppe Di Luca:** Writing – original draft, Investigation, Data curation. **Carlo Beatrice:** Writing – review & editing, Supervision, Project administration, Funding acquisition, Conceptualization. **Gabriele Di Blasio:** Writing – review & editing, Supervision, Methodology, Investigation, Data curation, Conceptualization.

Declaration of competing interest

The authors declare that they have no known competing financial interests or personal relationships that could have appeared to influence the work reported in this paper.

Data availability

Data will be made available on request.

Acknowledgments

This work is financially supported by MIUR - “Ministero dell’Istruzione dell’Università e della Ricerca” under project EXTREME - “Innovative technologies for EXTREMely Efficient spark ignited engines”, ARS01_00849. The authors would like to thank Mr. Sergio Stucchi, Mr. Marcello Gargano and Mr. Onofrio De Michele of the “Centro Ricerche Fiat” for the realization and support related to the supercritical water injection system, and Mr. Alessio Schiavone and Mr. Augusto Piccolo for their technical support in the engine assembly and testing.

Appendix A

Model set generation and selection procedure

The starting point for the generation of a set of model formulations is the null model (i.e., constant function). Then, various terms have been added, including fixed, mixed, and random effects terms, to explore all the possible and relevant combinations. The explanatory variables considered are the temperature, pressure, ET_W, and SOI_W. In merit to the temperature, different measurements have been used in an exclusive way. In particular, three different temperatures have been tested: the experimental T_{exp}, and the predicted ones by the heat transfer model at the injector inlet $T_{inj_{in}}$ and at the nozzle outlet $T_{inj_{out}}$. For multivariate models, the ET is always included in the formulation as it is the most relevant parameter for the injected mass in injector systems. Random effect terms regarding the experimental setup and operating point have been considered by adding two grouping variables. The experimental setup term is added since there was the need to change injector body and nozzles at different times. This term allows to consider a possible variability in the prototypal apparatus. Instead, the operating point term is added to account for the variation in-chamber conditions (i.e., back pressure) that influence the injector performance.

In *particular*, for clarity, the model set tested is reported synthetically in Table 7, adopting the Wilkinson nomenclature.

Table 7
Formulation adopted tested.

Null model: $m\ 1$
1 fixed effect model:
$m\ 1 + X$
with $X \in \{ET, T_\chi, SOI, p\}$, $\chi \in \{exp, inj_{in}, inj_{out}\}$
1 fixed effect, 1 mixed effect model:
$m\ 1 + X + Y{*}Z$,
with $X, Y, Z \in \{ET, T_\chi, SOI, p\}$, $\chi \in \{exp, inj_{in}, inj_{out}\}$, $Y \neq Z$
2 fixed effect model:
$m\ 1 + ET + X$,
with $X, Y, Z \in \{T_\chi, SOI, p\}$, $\chi \in \{exp, inj_{in}, inj_{out}\}$
2 fixed effect, 1 mixed effect model:
$m\ 1 + ET + X + Y{*}Z$,
with $X, Y, Z \in \{T_\chi, SOI, p\}$, $\chi \in \{exp, inj_{in}, inj_{out}\}$, $Y \neq Z$
2 fixed effect, 1 mixed effect, 1 random effect model:
$m\ 1 + ET + X + Y{*}Z + (1\|ExperimentalSetup)$,
with $X, Y, Z \in \{T_\chi, SOI, p\}$, $\chi \in \{exp, inj_{in}, inj_{out}\}$, $Y \neq Z$
2 fixed effect, 1 mixed effect, 1 random effect model:
$m\ 1 + ET + X + Y{*}Z + (1\|OP)$,
with $X, Y, Z \in \{T_\chi, SOI, p\}$, $\chi \in \{exp, inj_{in}, inj_{out}\}$, $Y \neq Z$
2 fixed effect, 1 mixed effect, 2 random effect model:
$m\ 1 + ET + X + Y{*}Z + (1\|ExperimentalSetup) + (1\|OP)$,
with $X, Y, Z \in \{T_\chi, SOI, p\}$, $\chi \in \{exp, inj_{in}, inj_{out}\}$, $Y \neq Z$
3 fixed effect, 1 mixed effect, 1 random effect model:
$m\ 1 + ET + X + W + Y{*}Z + (1\|ExperimentalSetup)$
with $W, X, Y, Z \in \{T_\chi, SOI, p\}$, $\chi \in \{exp, inj_{in}, inj_{out}\}$, $Y \neq Z, X \neq W$
3 fixed effect, 1 mixed effect, 1 random effect model:

(*continued on next page*)

Table 7 (*continued*)

$m\ 1 + ET + X + W + Y^{*}Z + (1\|OP)$,
with $W,X,Y,Z \in \{T_{\chi}, SOI, p\},\ \chi \in \{exp, inj_{in}, inj_{out}\},\ Y \neq Z, X \neq W$
3 fixed effect, 1 mixed effect, 2 random effect model:
$m\ 1 + ET + X + W + Y^{*}Z + (1\|ExperimentalSetup) + (1\|OP)$,
with $W,X,Y,Z \in \{T_{\chi}, SOI, p\},\ \chi \in \{exp, inj_{in}, inj_{out}\},\ Y \neq Z, X \neq W$

The *model* resulting in the best AIC, BIC, R^2_{adj}, and log likelihood includes 2 fixed effect, 1 mixed effect and 2 random effect terms.

Appendix B

In Table 8 a comparison is proposed to assess the relevance of the random effect "(1|ExperimentalSetup)". In Table 9 a comparison is proposed to assess the relevance of the adopted temperature with fixed model formulation.

Table 8
Comparison of the results of the best model with and without including the experimental setup configuration.

Metrics	Best model	Model without (1|ExperimentalSetup)
AIC	186.4	230.25
BIC	211.7	252.4
Adjusted R^2	0.834	0.741
Loglikelihood	−85.2	−108.12
Dispersion	0.357	0.438
Term		**p-value**
P	3.1e-3	1.0e-2
ET	5.8e-4	1.9e-2
Temperature	1.2e-12	6.96e-14
p*ET	7.6e-3	6.6e-2

Table 9
Comparison of the LME models using different temperatures.

Metrics	Model with $T_{inj,in}$	Model with $T_{inj,out}$	Model with T_{exp}
AIC	186.4	203.2	237.0
BIC	211.7	228.5	262.2
Adjusted R^2	0.834	0.818	0.776
Loglikelihood	−85.2	−93.6	−110.5
Dispersion	0.357	0.373	0.412
Term		**p-value**	
P	3.1e-3	2.8e-3	5.4e-3
ET	5.8e-4	4.2e-4	5.8e-3
Temperature	1.2e-12	6.6e-9	0.97
p*ET	7.6e-3	6.8e-3	2.0e-5

References

[1] K. Semkov, E. Mooney, M. Connolly, C. Adley, Efficiency improvement through waste heat reduction, Appl. Therm. Eng. 70 (1) (Sep. 2014) 716–722, https://doi.org/10.1016/j.applthermaleng.2014.05.030.

[2] O. Farhat, J. Faraj, F. Hachem, C. Castelain, M. Khaled, A recent review on waste heat recovery methodologies and applications: comprehensive review, critical analysis and potential recommendations, Clean. Eng. Technol. 6 (Feb. 2022) 100387, https://doi.org/10.1016/j.clet.2021.100387.

[3] C. Forman, I.K. Muritala, R. Pardemann, B. Meyer, Estimating the global waste heat potential, Renew. Sustain. Energy Rev. 57 (May 2016) 1568–1579, https://doi.org/10.1016/j.rser.2015.12.192.

[4] 'Lawrence Livermore National Laboratory. Energy Flow Charts: Charting the Complex Relationships among Energy.' Accessed: May 15, 2023. [Online]. Available: https://flowcharts.llnl.gov.

[5] G. Bianchi, et al., Estimating the waste heat recovery in the European Union industry, Energy Ecol. Environ. 4 (5) (Oct. 2019) 211–221, https://doi.org/10.1007/s40974-019-00132-7.

[6] N. Duarte Souza Alvarenga Santos, V. Rückert Roso, A. C. Teixeira Malaquias, and J. G. Coelho Baêta, 'Internal combustion engines and biofuels: Examining why this robust combination should not be ignored for future sustainable transportation', *Renew. Sustain. Energy Rev.*, vol. 148, p. 111292, Sep. 2021, doi: 10.1016/j.rser.2021.111292.

[7] E. Scolaro, M. Beligoj, M.P. Estevez, L. Alberti, M. Renzi, M. Mattetti, Electrification of agricultural machinery: a review, IEEE Access 9 (2021) 164520–164541, https://doi.org/10.1109/ACCESS.2021.3135037.

[8] C. A. Díaz González and L. Pacheco Sandoval, 'Sustainability aspects of biomass gasification systems for small power generation', *Renew. Sustain. Energy Rev.*, vol. 134, p. 110180, Dec. 2020, doi: 10.1016/j.rser.2020.110180.

[9] D. T. Hountalas, C. O. Katsanos, and V. T. Lamaris, 'Recovering Energy from the Diesel Engine Exhaust Using Mechanical and Electrical Turbocompounding', presented at the SAE World Congress & Exhibition, Apr. 2007, pp. 2007-01–1563. doi: 10.4271/2007-01-1563.

[10] S. Ahmadi Atouei, A. A. Ranjbar, and A. Rezania, 'Experimental investigation of two-stage thermoelectric generator system integrated with phase change materials', *Appl. Energy*, vol. 208, pp. 332–343, Dec. 2017, doi: 10.1016/j.apenergy.2017.10.032.

[11] P. Dimitriou, R. Burke, Q. Zhang, C. Copeland, and H. Stoffels, 'Electric Turbocharging for Energy Regeneration and Increased Efficiency at Real Driving Conditions', *Appl. Sci.*, vol. 7, no. 4, Art. no. 4, Apr. 2017, doi: 10.3390/app7040350.

[12] V. Pandiyarajan, M. Chinna Pandian, E. Malan, R. Velraj, and R. V. Seeniraj, 'Experimental investigation on heat recovery from diesel engine exhaust using finned shell and tube heat exchanger and thermal storage system', *Appl. Energy*, vol. 88, no. 1, pp. 77–87, Jan. 2011, doi: 10.1016/j.apenergy.2010.07.023.

[13] M. Güven, H. Bedir, G. Anlaş, Optimization and application of Stirling engine for waste heat recovery from a heavy-duty truck engine, Energy Convers. Manag. 180 (Jan. 2019) 411–424, https://doi.org/10.1016/j.enconman.2018.10.096.

[14] M. Brignone, A. Ziggiotti, Impact of novel thermoelectric materials on automotive applications, AIP Conf. Proc. 1449 (1) (Jun. 2012) 493–496, https://doi.org/10.1063/1.4731601.

[15] R. K. Stobart, A. Wijewardane, and C. Allen, 'The Potential for Thermo-Electric Devices in Passenger Vehicle Applications', presented at the SAE 2010 World Congress & Exhibition, Apr. 2010, pp. 2010-01–0833. doi: 10.4271/2010-01-0833.

[16] D. Di Battista, M. Mauriello, R. Cipollone, Waste heat recovery of an ORC-based power unit in a turbocharged diesel engine propelling a light duty vehicle, Appl. Energy 152 (Aug. 2015) 109–120, https://doi.org/10.1016/j.apenergy.2015.04.088.
[17] M. Costa, et al., Model based optimization of the control strategy of a gasifier coupled with a spark ignition engine in a biomass powered cogeneration system, Appl. Therm. Eng. 160 (Sep. 2019) 114083, https://doi.org/10.1016/j.applthermaleng.2019.114083.
[18] Q. Liu, M. Xie, J. Fu, J. Liu, B. Deng, Cylinder steam injection (CSI) for internal combustion (IC) engine waste heat recovery (WHR) and its application on natural gas (NG) engine, Energy 214 (Jan. 2021) 118892, https://doi.org/10.1016/j.energy.2020.118892.
[19] J.C. Conklin, J.P. Szybist, A highly efficient six-stroke internal combustion engine cycle with water injection for in-cylinder exhaust heat recovery, Energy 35 (4) (2010) 1658–1664.
[20] Z. Wu, X. Yu, L. Fu, J. Deng, and L. Li, 'Experimental study of the effect of water injection on the cycle performance of an internal-combustion Rankine cycle engine', *Proc. Inst. Mech. Eng. Part J. Automob. Eng.*, vol. 228, no. 5, pp. 580–588, Apr. 2014, doi: 10.1177/0954407013511069.
[21] Q. Liu, J. Fu, Z. Liu, J. Liu, An approach for waste heat recovery of internal combustion engine: in-cylinder steam-air expansion, Appl. Therm. Eng. 197 (Oct. 2021) 117394, https://doi.org/10.1016/j.applthermaleng.2021.117394.
[22] I. Pioro, S. Mokry, I. Pioro, S. Mokry, 'Thermophysical properties at critical and supercritical pressures', in *heat transfer - theoretical analysis, Experimental investigations and industrial systems*, IntechOpen (2011), https://doi.org/10.5772/13790.
[23] A. Cantiani, A. Viggiano, and V. Magi, 'A CFD Model of Supercritical Water Injection for ICEs as Energy Recovery System', SAE International, Warrendale, PA, SAE Technical Paper 2020-37–0001, Jun. 2020. doi: 10.4271/2020-37-0001.
[24] A. Montanaro, L. Allocca, S. Ranieri, C. Beatrice, Computational-Experimental framework for realizing a novel Apparatus for supercritical water by induction heating, Heat Transf. Eng. 44 (9) (May 2023) 785–802, https://doi.org/10.1080/01457632.2022.2093531.
[25] X. Wu, et al., Numerical simulation of lean premixed combustion characteristics and emissions of natural gas-ammonia dual-fuel marine engine with the pre-chamber ignition system, Fuel 343 (Jul. 2023) 127990, https://doi.org/10.1016/j.fuel.2023.127990.
[26] S. Mokry, I. Pioro, P. Kirillov, Y. Gospodinov, Supercritical-water heat transfer in a vertical bare tube, Nucl. Eng. Des. 240 (3) (Mar. 2010) 568–576, https://doi.org/10.1016/j.nucengdes.2009.09.003.
[27] T. Gallaway, S.P. Antal, M.Z. Podowski, Multi-dimensional model of fluid flow and heat transfer in generation-IV supercritical water reactors, Nucl. Eng. Des. 238 (8) (Aug. 2008) 1909–1916, https://doi.org/10.1016/j.nucengdes.2007.11.019.
[28] Y.-Y. Yan, H.-C. Lio, T.-F. Lin, Condensation heat transfer and pressure drop of refrigerant R-134a in a plate heat exchanger, Int. J. Heat Mass Transf. 42 (6) (Mar. 1999) 993–1006, https://doi.org/10.1016/S0017-9310(98)00217-8.
[29] J.W.R. Peeters, M. Rohde, A heat transfer - friction analogy for fluids at supercritical pressure, J. Supercrit. Fluids 150 (Aug. 2019) 75–85, https://doi.org/10.1016/j.supflu.2019.03.009.
[30] T. Liu *et al.*, 'Operation Characteristics and Transient Simulation of an ICE-ORC Combined System', *Appl. Sci.*, vol. 9, no. 8, Art. no. 8, Jan. 2019, doi: 10.3390/app9081639.
[31] W. Wagner, A. Pruß, The IAPWS formulation 1995 for the thermodynamic properties of ordinary water substance for general and scientific use, J. Phys. Chem. Ref. Data 31 (2) (2002) 387–535.
[32] International Association for the Properties of Water and Steam, 'IAPWS R6-95 (2018), Revised Release on the IAPWS Formulation 1995 for the Thermodynamic Properties of Ordinary Water Substance for General and Scientific Use', 2018.
[33] T. J. Wolery, 'H2OI95: A Stand-Alone Fortran Code for Evaluating the IAPWS-95 Equation-of-State Model for Water (Rev. 1)', Lawrence Livermore National Lab. (LLNL), Livermore, CA (United States), 2020.
[34] P. Linstorm, NIST chemistry webbook, NIST standard reference database number 69, J Phys Chem Ref Data Monogr. 9 (1998) 1–1951.
[35] A. L. Oberg and D. W. Mahoney, 'Linear Mixed Effects Models', in *Topics in Biostatistics*, W. T. Ambrosius, Ed., in Methods in Molecular Biology^{TM}. , Totowa, NJ: Humana Press, 2007, pp. 213–234. doi: 10.1007/978-1-59745-530-5_11.
[36] J. C. Pinheiro and D. M. Bates, Eds., 'Linear Mixed-Effects Models: Basic Concepts and Examples', in *Mixed-Effects Models in S and S-PLUS*, in Statistics and Computing. , New York, NY: Springer, 2000, pp. 3–56. doi: 10.1007/0-387-22747-4_1.
[37] H. Akaike, A new look at the statistical model identification, IEEE Trans. Autom. Control 19 (6) (Dec. 1974) 716–723, https://doi.org/10.1109/TAC.1974.1100705.
[38] E. W. Lemmon, M. L. Huber, and M. O. McLinden, 'NIST standard reference database 23', *Ref. Fluid Thermodyn. Transp. Prop. REFPROP Version*, vol. 9, 2010.
[39] R. Zhao, Z. Zhang, W. Zhuge, Y. Zhang, Y. Yin, Comparative study on different water/steam injection layouts for fuel reduction in a turbocompound diesel engine, Energy Convers. Manag. 171 (Sep. 2018) 1487–1501, https://doi.org/10.1016/j.enconman.2018.06.084.
[40] A. Cantiani, A. Viggiano, and V. Magi, 'On the Direct Injection of Supercritical and Superheated H_2O into ICEs: The Role of the Injector Geometry', presented at the CO2 Reduction for Transportation Systems Conference, Jun. 2022, pp. 2022-37–0002. doi: 10.4271/2022-37-0002.
[41] F. Bedford, C. Rutland, P. Dittrich, A. Raab, F. Wirbeleit, Effects of direct water injection on DI diesel engine combustion, SAE Technical Paper (2000).
[42] E. Arabaci, Y. İçingür, H. Solmaz, A. Uyumaz, E. Yilmaz, Experimental investigation of the effects of direct water injection parameters on engine performance in a six-stroke engine, Energy Convers. Manag. 98 (Jul. 2015) 89–97, https://doi.org/10.1016/j.enconman.2015.03.045.